Research Square

Preprints are preliminary reports that have not undergone peer review.
They should not be considered conclusive, used to inform clinical practice,
or referenced by the media as validated information.

Mesenchymal Stromal Cell Sheet Transplantation Modulates Subacute Microglial States and Hindlimb Movement Patterns After Spinal Cord Injury

Kensuke Toriumi
Kindai University
Atsutoshi Ikeda
Kindai University
Tatsufumi Mori
Kindai University
Hiroki Tan
Kindai University
Shintaro Maeda
Kindai University
Toshiyuki Takehara
Kindai University Hospital
Koji Goto
Kindai University
Takeshi Teramura
teramura@med.kindai.ac.jp

Kindai University Hospital

Short Report

Keywords: spinal cord injury, mesenchymal stromal cells, cell sheet, microglia, P2RY12, TGF-β2, optical flow, locomotor analysis

Posted Date: November 24th, 2026

DOI: https://doi.org/10.21203/rs.3.rs-11588058/v1

License: This work is licensed under a Creative Commons Attribution 4.0 International License.
Read Full License

Additional Declarations: No competing interests reported.

Abstract

Background

Spinal cord injury (SCI) causes persistent neurological dysfunction, and effective regenerative treatments remain limited. Although mesenchymal stromal cell (MSC) transplantation is a promising therapeutic approach, its effects on the temporal dynamics of microglial phenotypes and their association with functional recovery remain unclear.

Methods

SCI was induced by forceps compression at the first lumbar vertebral level in male ICR mice, with or without concomitant MSC sheet transplantation. Microglial populations were characterized by flow cytometry using CD11b, P2RY12, and CD45, followed by microarray analysis and quantitative PCR of sorted $CD11b^{+}$ $CD45^{low}$ $P2RY12^{+}$ cells. Hindlimb movements were assessed 2 weeks after injury using ventral video imaging and optical flow analysis.

Results

At 48 h after injury, nearly all $CD11b^{+}$ $P2RY12^{+}$ cells exhibited high CD45 expression. In untreated mice, the proportion of $CD45^{low}$ population recovered to approximately 55% of the total $CD11b^{+}$ $P2RY12^{+}$ and remained at this level for up to 2 weeks, accompanied by sustained expression of injury-associated genes and reduced expression of homeostatic genes and Tgfb2. MSC sheet transplantation significantly increased the proportion of $CD45^{low}$ $P2RY12^{+}$ population and was associated with restoration of *Tgfb2* expression. Although transplantation did not significantly alter locomotor speed or hindlimb movement magnitude, it improved the alignment of hindlimb movements with the direction of travel and restored their frame-to-frame continuity, producing movement patterns resembling those of uninjured mice.

Conclusions

MSC sheet transplantation was associated with a shift toward a homeostatic microglial phenotype and restoration of *Tgfb2* expression following SCI, accompanied by improvements in hindlimb movement directionality and continuity. These findings suggest that qualitative aspects of motor recovery may not be adequately captured by conventional locomotor measures.

BACKGROUND

Spinal cord injury (SCI) remains a major global health challenge. It affects more than 15 million people worldwide and frequently results in permanent motor, sensory and autonomic dysfunction [1, 2]. Despite

advances in acute management, including surgical decompression and supportive care, treatments that can restore damaged neural tissue and neurological function remain limited [3, 4]. The limited regenerative capacity of the central nervous system is a major obstacle to functional recovery after SCI.

Mesenchymal stromal cells (MSCs) have attracted considerable interest as a potential therapy for SCI because of their immunomodulatory, angiogenic and neurotrophic properties [5]. Preclinical studies have shown beneficial effects of MSC transplantation on neurological recovery, and several clinical studies have reported improvements in sensory and motor function [6]. A recent network meta-analysis of 18 clinical studies also suggested improvements in motor function, sensory function and activities of daily living after MSC transplantation [7].

In Japan, an autologous MSC product for SCI, which received conditional and time-limited approval in 2018 [8], was recommended for full approval by the regulatory advisory committee in October 2026. However, the clinical efficacy of MSC-based therapies remains uncertain, and further preclinical studies are needed to clarify their mechanisms of action. Increasing evidence suggests that the therapeutic effects of MSCs are mediated, at least in part, by interactions with immune cells. MSC transplantation after SCI shifts macrophages toward an alternatively activated phenotype, accompanied by reduced scarring and improved locomotor recovery [9]. After SCI, resident microglia undergo substantial phenotypic and functional changes and contribute to both inflammatory responses and tissue repair [10, 11]. In the healthy CNS, microglial identity and homeostasis depend on TGF-β signaling [12, 13], and MSC-derived factors suppress microglial inflammatory responses in a TGF-β-dependent manner in vitro [14]. Nevertheless, how MSC transplantation affects the temporal dynamics of microglial states after SCI—in particular, their return from an activated to a homeostatic state—remains poorly understood, and the relationship between these cellular changes and functional outcomes has not been fully elucidated.

Objective and quantitative assessment of locomotor function is also essential for evaluating therapeutic effects in experimental SCI. Conventional scoring systems may not fully capture subtle changes in locomotor patterns, such as involuntary or non-propulsive movements. To address this limitation, we used a quantitative locomotor analysis system based on RGB-D video imaging combined with optical flow analysis. By separating whole-body translocation from local hindlimb movement, this approach characterizes the spatial and directional components of movement and may provide information beyond that obtained with conventional locomotor assessments.

In this study, we tracked the temporal changes in microglial phenotypes after SCI in mice, using CD45 and P2RY12 expression to distinguish homeostatic, intermediate and activated states, and examined how MSC sheet transplantation affects these dynamics. We also assessed locomotor outcomes using quantitative optical flow analysis. By integrating cellular and behavioral analyses, we aimed to gain further insight into the mechanisms underlying MSC-based therapy for SCI.

METHODS

Ethical Consideration for animal studies

All procedures related to animal handling, care, surgery, and sacrifice were approved by the Institutional Animal Care and Use Committee of Kindai University as the approved research project number KAME2024-039 and performed in accordance with institutional guidelines and regulations. All methods are reported in accordance with ARRIVE guidelines.

Preparation of mouse bone marrow mesenchymal stromal cells (BMMSCs)

Mouse BMMSCs were isolated as previously described [15]. Briefly, femurs and tibias were harvested from 10-week-old male ICR mice, cleaned of surrounding soft tissues, cut into small pieces, and digested with 0.1% collagenase type II (FUJIFILM Wako Pure Chemical Corporation, Tokyo, Japan) for 30 minutes. Single-cell suspensions containing BMMSCs were collected, washed twice with PBS, and plated on cell culture dishes (Sumilon, Sumitomo Bakelite Co. Ltd., Tokyo, Japan) in αMEM (Thermo Fisher Scientific, Waltham, MA, USA) supplemented with 200 mM L-glutamine and 10% fetal bovine serum (CORNING, Lowell, MA, USA) under 5% CO2 and 5% O2 at 37°C. The following day, the medium was replaced to remove dead cells and debris. After 10 days of culture, BMMSCs were detached using TrypLE (Thermo Fisher Scientific) for further experiments. BMMSCs within three passages were used in the experiment.

Spinal cord injury model

Ten-week-old male ICR mice were anesthetized with inhaled sevoflurane. A 6–8 mm midline skin incision was made over the back, the upper half of the L1 lamina was removed, and the exposed spinal cord was compressed with fine-tipped forceps to produce the spinal cord injury (SCI). The injury site was confirmed by micro-CT (CosmoScan GX II, Rigaku Corporation, Tokyo, Japan). Before the study, the operator was trained to apply a consistent compression using forceps fitted with a pressure sensor. The compression force was 0.13 ± 0.03 N and the compression time was 3.25 ± 0.25 s (mean ± SD)

In the cell transplantation group, bone marrow-derived MSCs (BMMSCs) at passage ≤ 3 were formed into cell sheets to keep the number of transplanted cells constant, and a sheet was placed directly onto the injured spinal cord. To prepare the sheets, 2×10^5 cells were seeded into temperature-responsive poly(N-isopropylacrylamide) (PIPAAm)-grafted 24-well plates (UpCell, CellSeed Inc., Tokyo, Japan) 24 h before transplantation. Just before transplantation, the medium was replaced with PBS and the plates were left at 20°C for 10 min to detach the cell sheet.

After transplantation, the fascia and skin were sutured to prevent cerebrospinal fluid leakage. Mice were returned to individual cages once they had recovered from anesthesia.

Video acquisition and whole-body locomotor speed

Spontaneous locomotion was recorded from the ventral side as mice walked along a transparent acrylic walkway (Supplementary Fig. 1). A spatial calibration factor (cm/pixel) was determined for each video using the known walkway width, allowing pixel displacements to be converted into physical distances. All image processing was performed using OpenCV. A region of interest (ROI) encompassing the mouse was manually initialized and subsequently tracked using the channel and spatial reliability tracking (CSRT) algorithm. Whole-body velocity was calculated from the frame-to-frame displacement of the ROI center along the longitudinal axis of the walkway, multiplied by the spatial calibration factor and frame rate, and expressed in cm/s, with forward movement defined as positive. Mean locomotor speed was calculated for each mouse using frames with forward velocities ≥ 2 cm/s, excluding stationary and backward-moving frames. The tracked ROIs were cropped to generate image sequences for subsequent hindlimb analysis.

Quantification of hindlimb movement

Consecutive cropped images were registered using the enhanced correlation coefficient (ECC) algorithm with a translation-only model to minimize residual positional shifts after whole-body tracking. Images were converted to grayscale and normalized for brightness to reduce interframe illumination differences. Contrast-limited adaptive histogram equalization (CLAHE) was then applied to enhance local image features for motion estimation. An analysis ROI encompassing both hindlimbs was manually defined. Dense optical flow was calculated using the Farnebäck algorithm to estimate pixel displacements between consecutive frames. The image axes were aligned with the walkway, with the X component representing the direction of travel (forward positive) and the Y component representing the lateral direction.

Morphological opening and closing were applied to remove small isolated regions and fill gaps within detected regions, respectively. The largest contour was selected, and its convex hull was used to define a mask encompassing the principal motion region. Optical-flow vectors within this mask were spatially averaged for the X and Y components separately and expressed in pixels/frame. These signed components represent net local hindlimb motion relative to the body after tracking and registration. Because opposing movements of the left and right hindlimbs may cancel during spatial averaging, the resulting vectors do not represent total hindlimb movement magnitude. The Y component primarily reflects net lateral motion within the hindlimb region.

Whole-body and hindlimb movement indices

Three indices were calculated for each mouse from the frame-by-frame hindlimb displacement vectors (X and Y, pixels/frame).

The forward–backward share was defined as $\Sigma X^2 / \Sigma(X^2 + Y^2) \times 100$, representing the proportion of squared motion components aligned with the direction of travel. The movement orientation angle was defined as the angle between the direction of travel and the major axis of the X–Y displacement

distribution. The major axis was determined by principal component analysis of the X–Y covariance matrix, and the angle was expressed within a range of 0–90°. Smaller angles indicate a predominant alignment of hindlimb motion with the direction of travel.

The jitter index was defined as mean |X(t + 1) − X(t)| / mean |X(t)|, where t and t + 1 denote consecutive frames. Lower values indicate greater frame-to-frame continuity of the longitudinal hindlimb motion component, whereas higher values reflect greater temporal fluctuations. For independent, zero-mean Gaussian fluctuations, the expected value of this index is √2 (approximately 1.41).

Tissue harvest and cell isolation

Ten-week-old male ICR mice were euthanized, and the injured spinal cord was harvested. A 4-mm segment centered on the injury site was removed together with the vertebrae and used either for formalin fixation or for cell isolation. For cell isolation, the tissue was finely minced with surgical scissors and digested with 0.1% collagenase type II for 30 min at 37°C. The cell suspension was passed through a 40-μm cell strainer to remove debris and washed twice with PBS. Cells were then incubated with fluorochrome-conjugated antibodies against CD11b, CD45 and P2RY12 (Supplementary table 1) for 30 min at 4°C with gentle agitation, and washed twice with PBS containing 2% fetal calf serum (FCS).

Transcriptomic analysis using Clariom™ S Pico Assay

Total RNA was extracted from FACS-sorted cell fractions using TRIzol reagent (Thermo Fisher Scientific, Waltham, MA, USA) according to the manufacturer's instructions. Transcriptome profiling was performed using the Clariom™ S Pico Assay HT, mouse kit (Thermo Fisher Scientific) following the manufacturer's protocol. Briefly, low-input RNA was subjected to reverse transcription, cDNA amplification, and fragmentation, followed by labeling and hybridization to Clariom S mouse arrays. After hybridization, arrays were washed, stained, and scanned using the GeneChip™ Scanner system (Thermo Fisher Scientific). Raw data were processed using Transcriptome Analysis Console (TAC) software (Thermo Fisher Scientific). Gene expression levels were normalized using the SST-RMA algorithm. Differentially expressed genes were identified based on fold-change thresholds and statistical significance.

Histology and immunohistochemistry

The spinal cord was harvested together with the vertebral column and immediately fixed in 10% neutral buffered formalin. The fixative was replaced with fresh solution after 48 h, and fixation was continued for a total of 5 days. Samples were then decalcified in KCX (Falma Co., Ltd., Tokyo, Japan) for 72 h and embedded in paraffin. Sagittal sections (4 μm thick) were cut on a sliding microtome (Sakura Finetek Japan, Tokyo, Japan). After deparaffinization, sections were stained with hematoxylin and eosin (HE) and with Luxol Fast Blue (LFB) for myelin.

For immunohistochemistry, deparaffinized sections were subjected to antigen retrieval in citrate buffer (pH 6.0) at 95°C for 20 min, and endogenous peroxidase activity was quenched with 3% H_2O_2 for 10 min. After blocking with 1% Block Ace (DS Pharma Biomedical Co., Ltd., Osaka, Japan), sections were incubated overnight at 4°C with an anti-P2RY12 antibody (Supplementary table 1) diluted 1:50 in PBS containing 1% Block Ace. After three washes in PBS, sections were incubated with an HRP-conjugated secondary antibody (1:500) for 30 min at room temperature. After three further washes in PBS, signals were developed with DAB (Peroxidase Stain DAB Kit, nacalai) and the sections were counterstained with hematoxylin.

Quantitative RT-PCR

Total RNA was extracted from specimens using TRI Reagent® (Molecular Research Center Inc., Cincinnati, OH, USA) and reverse-transcribed using the PrimeScript® RT Master Mix Kit (TAKARA Bio Inc., Shiga, Japan). Quantitative real-time PCR (qPCR) was performed using Perfect Real-Time SYBR Green II (TAKARA) with gene-specific primers listed in supplementary table 2. To avoid amplification of contaminating genomic DNA, all primer pairs were designed to span at least one intron. Relative gene expression levels were normalized to *Actb* as an internal control and calculated using the $2^{-\Delta\Delta Ct}$ method.

Statistical analysis

The experimental unit was the individual mouse. Except for the longitudinal assessment of locomotor speed in SCI mice (Fig. 1C), each data point represents an independent biological sample from a separate animal, and samples were not pooled. Group sizes were n = 3 per group for qPCR and FACS, and n = 3 (Control), 6 (SCI), and 6 (SCI + TP) for behavioral analysis. Data are presented as mean ± SD. Microarray analysis was performed with one array per condition and was treated as exploratory: no statistical testing was applied, and candidate genes were selected for qPCR validation based on fold change ($|\log2FC| \geq 1$) and expression level ($\log2 \geq 7$). qPCR data among the three groups (Control, SCI 2 wk, and SCI + TP 2 wk) were compared by one-way ANOVA followed by Tukey's multiple comparison test.

Locomotor speed was compared by one-way ANOVA followed by Tukey's test; in Fig. 1C, SCI mice assessed at 1 and 2 weeks were the same animals, and the two time points were treated as separate groups. Hindlimb movement indices were compared among the three groups by one-way ANOVA followed by Tukey's test. In addition, because the primary question was the effect of MSC transplantation, two planned comparisons were performed: SCI vs SCI + TP (treatment effect) and Control vs SCI (injury-induced deficit, with controls serving as a reference). Each planned comparison used a two-sided Welch's t-test, and P values were adjusted for the two comparisons by the Holm method. qPCR and FACS data were analyzed with JMP 8.0 (SAS Institute Inc., Cary, NC, USA), and behavioral data were analyzed with Python 3.13 using SciPy 1.18 and NumPy 2.5. $P < 0.05$ was considered statistically significant. Mice showing abnormal behavior unrelated to the injury (e.g., avoidance behavior) were excluded by blinded video review before analysis.

Use of generative artificial intelligence

Claude Opus 5.5 (Anthropic, San Francisco, CA, USA), a large language model, was used in October 2026 to assist with re-analyses of processed data, figure preparation in R and Python, English-language proofreading, and independent verification of statistical calculations manually performed by the authors. All analyses, results and text were reviewed and verified by the authors, who take full responsibility for the content of this article.

Establishment and characterization of a mouse model of spinal cord injury induced by forceps compression

A mouse model of spinal cord injury (SCI) was established in 10-week-old male ICR mice by partial removal of the lamina of the first lumbar vertebra (L1), followed by compression of the exposed spinal cord using fine-tipped forceps (Fig. 1A). Histological examination at 96 h after injury revealed hemorrhage and clot formation at the lesion epicenter on hematoxylin and eosin (H&E) staining, together with demyelination on Luxol fast blue (LFB) staining. Demyelination persisted or expanded through 2 weeks after SCI, the final observation time point of this study (Fig. 1B).

Whole-body locomotor speed was markedly reduced at 1 week after SCI (Control, 14.8 ± 3.8 cm/s; SCI 1 wk, 5.8 ± 1.4 cm/s; $P < 0.001$, Tukey's test) and remained significantly lower than that of controls at 2 weeks (SCI 2 wk, 9.0 ± 2.4 cm/s; $P = 0.012$). Although locomotor speed tended to increase between 1 and 2 weeks, the difference was not statistically significant ($P = 0.097$; Fig. 1C).

Representative movement traces from a control mouse showed that the amplitude of the forward (X) component of hindlimb motion varied with whole-body locomotor speed. Larger excursions were observed during faster locomotion, whereas hindlimb motion was reduced when locomotion nearly stopped (frames ~ 50–95; Fig. 1D). In contrast, at 2 weeks after SCI, whole-body locomotor speed remained low, and the X component exhibited persistent, small-amplitude fluctuations even during periods of minimal forward movement.

SCI induces CD45 upregulation in microglia and persistent expression of disease-associated microglial genes

We next examined changes in microglial phenotypes following SCI using flow cytometry. In the spinal cord of uninjured mice, nearly all P2RY12^{+} cells exhibited a CD45^{low} phenotype characteristic of homeostatic microglia. At 48 h after SCI, nearly all P2RY12^{+} cells were classified into the CD45^{high} population. By 96 h, approximately 55% of P2RY12^{+} cells were classified into the CD45^{low} population, and this proportion remained largely unchanged at 2 weeks (Fig. 2A).

Immunohistochemical staining for P2RY12 revealed no substantial changes in the overall number of P2RY12^{+} cells following SCI. However, their spatial distribution varied over time. At 96 h after injury, P2RY12^{+} cells were predominantly concentrated near the lesion site, whereas at 2 weeks, they were more diffusely distributed around the demyelinated area (Fig. 2B).

To further characterize the transcriptional changes in microglia, CD11b^{+}P2RY12^{+}CD45^{low} cells, a population enriched in homeostatic microglia, were isolated by fluorescence-activated cell sorting and subjected to microarray analysis. In uninjured mice, this population exhibited a characteristic homeostatic microglial gene expression profile compared with the CD11b^{+}CD45^{+} population. Using the uninjured population as a reference, we compared the transcriptional profiles at 96 h and 2 weeks after SCI. The gene expression profile at 2 weeks was more similar to that of uninjured microglia than the profile at 96 h, as indicated by a reduction in the root mean square (RMS) distance from 1.89 to 1.23. Nevertheless, the CD45^{low} population at 2 weeks continued to exhibit elevated expression of disease-associated microglia (DAM)-related genes, including *Igf1* and *Gpnmb*, which have been implicated in neuroprotection and tissue repair. In contrast, the expression of homeostatic microglial markers, including *Tmem119* and *Sall1*, as well as *Tgfb2*, remained reduced (Fig. 2C).

MSC sheet transplantation increases the proportion of CD45-low microglia and restores Tgfb2 and Id3 expression following SCI

In mice receiving mesenchymal stromal cell (MSC) sheet transplantation at the injury site, the expansion of the LFB-negative demyelinated area tended to be attenuated compared with untreated SCI mice (Fig. 3A). In contrast, no substantial differences were observed in the overall number or spatial distribution of P2RY12^{+} cells (Fig. 3B).

Flow cytometric analysis demonstrated that the proportion of CD45^{low} cells within the P2RY12^{+} population increased to approximately 81% at 1 week and 90% at 2 weeks after SCI in MSC-treated mice, compared with approximately 58% in untreated SCI mice (Fig. 3C and 3D). We subsequently compared the gene expression profiles of the sorted CD45^{low} population using microarray analysis. The expression of *Tgfb2*, which was reduced at 2 weeks after SCI, was restored to a level approaching that of uninjured controls following MSC transplantation. The expression of *Id3*, a downstream target of TGF-β/BMP signaling, and *Il10*, an anti-inflammatory cytokine, was also increased (Supplementary Fig. 2). In contrast, no substantial differences were observed in the expression of conventional homeostatic microglial markers.

Given the variability in injury severity among individual mice, we performed quantitative real-time PCR (qPCR) using CD11b^{+}P2RY12^{+}CD45^{low} cells independently isolated from three mice per group (uninjured controls, SCI at 2 weeks, and SCI with MSC transplantation at 2 weeks). The expression levels of *Tgfb2* and *Id3* were significantly higher in the MSC-treated group than in the untreated SCI group. *Igf1* expression was higher in the MSC-treated group than in uninjured controls, whereas *Gpnmb* expression showed considerable interindividual variability, with no significant differences among groups (Fig. 3E).

MSC sheet transplantation improves the directionality and temporal continuity of hindlimb movement after SCI

At 2 weeks after injury, whole-body locomotor speed was significantly lower in both SCI and SCI + TP mice than in controls (P = 0.018 and P = 0.007, respectively; Tukey's test), with no significant difference between SCI and SCI + TP mice (P = 0.79; Fig. 4A). Analysis of hindlimb motion vectors revealed no significant differences among groups in the standard deviations of the longitudinal (X) and lateral (Y) components or in the mean magnitude of the motion vectors (all pairwise P ≥ 0.08, Tukey's test). However, the distributions of hindlimb motion vectors showed distinct patterns. In SCI mice, the vectors were distributed approximately isotropically around the origin, whereas those in control and SCI + TP mice showed an elongated distribution along the direction of travel (X axis) (Fig. 4C).

The forward–backward share of hindlimb movement was significantly lower in SCI mice than in controls (54.7 ± 7.4% vs. 72.8 ± 6.9%; P = 0.007, Tukey's test; Fig. 4B). SCI mice also exhibited a larger angle between the major axis of the motion vector distribution and the direction of travel (29.1 ± 20.7° vs. 5.8 ± 7.4°; Fig. 4D), together with a higher jitter index (1.45 ± 0.08 vs. 1.23 ± 0.07; Holm-adjusted P = 0.015, planned comparison; Fig. 4E), indicating greater frame-to-frame variability in the longitudinal component of hindlimb movement.

MSC sheet transplantation significantly increased the forward–backward share (63.8 ± 6.2%; Holm-adjusted P = 0.044 vs. SCI), reduced the movement orientation angle (6.0 ± 5.4°; P = 0.037 vs. SCI, Tukey's test), and decreased the jitter index (1.24 ± 0.19; Holm-adjusted P = 0.048 vs. SCI). These changes indicate improved directionality and temporal continuity of hindlimb movement following MSC transplantation, despite the absence of a significant improvement in whole-body locomotor speed.

Discussion

In this study, we investigated the temporal changes in microglial populations following spinal cord injury (SCI) and the effects of mesenchymal stromal cell (MSC) sheet transplantation on microglial phenotypes and locomotor function.

At 48 h after SCI, nearly all P2RY12^{+} cells exhibited high CD45 expression. In untreated mice, the proportion of P2RY12^{+} CD45^{low} cells subsequently increased to approximately 55% and remained at this level through 2 weeks. In contrast, MSC-treated mice showed an increase in the P2RY12^{+} CD45-intermediate population at 96 h, followed by an increase in the P2RY12^{+} CD45^{low} population to approximately 80% at 1 week and 90% at 2 weeks. These findings suggest that MSC transplantation may influence the subsequent evolution of microglial phenotypes rather than suppress the initial injury-associated response. Notably, the spontaneous increase in CD45^{low} cells in untreated mice did not indicate complete restoration of a homeostatic transcriptional profile. Although their overall transcriptional profile at 2 weeks more closely resembled that of uninjured microglia, homeostatic genes, including *Tmem119* and *Sall1*, remained downregulated, whereas injury-associated genes, such as *Igf1* and *Gpnmb*, remained elevated. *Tgfb2* expression also remained low. Thus, changes in CD45-defined populations and recovery of homeostatic transcriptional programs do not necessarily occur in parallel following SCI.

TGF-β signaling plays a critical role in maintaining microglial identity and homeostatic transcriptional programs [12]. MSC transplantation increased *Tgfb2* expression in $CD45^{low}$ cells toward levels observed in uninjured mice, accompanied by increased *Id3* expression. ID3 is a transcriptional regulator responsive to TGF-β/BMP signaling and has been implicated in the differentiation and maintenance of tissue-resident macrophages [16] and macrophage polarization [17]. Although its role in microglia remains incompletely understood, these findings suggest that MSC transplantation may modulate transcriptional programs associated with microglial identity and immune regulation.

The effects of TGF-β2 following central nervous system injury are context-dependent. Previous studies have associated TGF-β2 with scar formation after SCI [18], neuronal survival [19, 20], and enhanced neuronal responsiveness to neurotrophic factors [21]. Conversely, TGF-β2 can promote glial and fibrotic scarring, and its neutralization has been reported to attenuate scar formation without consistently improving axonal regeneration [22–24]. Thus, increased *Tgfb2* expression should not be interpreted as uniformly beneficial. Our findings identify $CD45^{low}$ cells as a potential cellular compartment in which *Tgfb2* expression is modulated following MSC transplantation, consistent with previous reports of TGF-β-dependent immunomodulatory effects of MSC-derived factors [9, 14].

MSC transplantation was also associated with elevated *Igf1* expression relative to uninjured controls, while exploratory microarray analysis suggested increased *Il10* expression. Microglia-derived IGF-1 has been implicated in neuronal survival and myelination [25, 26], whereas IL-10 can suppress inflammatory responses and support neuronal survival [27]. However, increased expression of inflammatory mediators, including *Il6*, was also observed. IL-6 has context-dependent effects following SCI, with reported roles in both tissue injury and axonal regeneration [28]. Therefore, the transcriptional changes associated with MSC transplantation cannot be interpreted simply as a shift toward an anti-inflammatory phenotype. The concurrent expression of protective and inflammatory mediators may reflect heterogeneous microglial populations or transitional states, which require further investigation at the single-cell level.

Locomotor analysis revealed additional effects of MSC transplantation that were not detected by conventional movement measures. Although previous clinical studies have reported neurological improvements following MSC administration in patients with SCI [8], differences in experimental conditions and outcome measures limit direct comparisons. In our study, MSC transplantation did not significantly improve whole-body locomotor speed or the magnitude of net hindlimb movement at 2 weeks. In contrast, the forward–backward share, movement orientation angle, and jitter index indicated improvements in the directionality and temporal continuity of hindlimb movement. These findings suggest that MSC transplantation may improve certain qualitative aspects of hindlimb movement without restoring overall locomotor performance. The observed changes may reflect partial recovery of organized motor activity, although their physiological significance remains uncertain. Because these indices were derived from exploratory two-dimensional video analysis in a small cohort, further validation using established behavioral scales and detailed kinematic assessments is warranted.

Several mechanisms may contribute to these changes in hindlimb movement. Impaired inhibitory neurotransmission associated with reduced neuronal KCC2 expression has been implicated in spasticity following SCI [29], while microglia-derived BDNF can modulate neuronal KCC2 expression and spinal excitability [30]. Microglial activation has also been associated with neuropathic pain after SCI [31], and MSC transplantation has been reported to alleviate pain-related behaviors in experimental models [32]. Although these mechanisms may contribute to altered locomotor patterns, the present study does not establish a causal relationship between microglial modulation and functional improvement.

Several limitations should be acknowledged. First, the study was restricted to a single SCI model and a 2-week observation period. Second, CD11b, P2RY12, and CD45 expression cannot completely distinguish resident microglia from infiltrating monocyte-derived macrophages, and changes in population proportions do not establish transitions at the individual-cell level. Third, increased *Tgfb2* and *Id3* expression does not demonstrate activation or causal involvement of TGF-β signaling. Finally, the physiological basis of the observed improvements in hindlimb movement remains unclear. Additional behavioral, electrophysiological, and mechanistic studies are required to determine whether these changes reflect altered spinal excitability, pain-related behavior, or partial recovery of motor control.

Conclusions

MSC sheet transplantation increased the proportion of $CD45^{low}$ cells among $P2RY12^{+}$ cells and was associated with increased *Tgfb2* and *Id3* expression following SCI. These cellular changes were accompanied by improvements in the directionality and temporal continuity of hindlimb movement, despite no significant improvement in whole-body locomotor speed. These findings suggest that MSC transplantation may modulate microglial responses during the subacute phase of SCI and improve aspects of locomotor function not captured by conventional measures of locomotion. Further mechanistic and longitudinal studies are warranted to clarify the relationship between microglial modulation and functional recovery.

Abbreviations

CLAHE
Contrast-limited adaptive histogram equalization
CSRT
Channel and spatial reliability tracking
DAB
3,3'-Diaminobenzidine
DAM
Disease-associated microglia
ECC
Enhanced correlation coefficient
FACS

Fluorescence-activated cell sorting
FCS
Fetal calf serum
IGF-1
Insulin-like growth factor 1
LFB
Luxol Fast Blue
MSC
Mesenchymal stromal cell
P2RY12
Purinergic receptor P2Y12
qPCR
Quantitative polymerase chain reaction
RMA
Robust multi-array average
ROI
Region of interest
SCI
Spinal cord injury
TP
Transplantation

Declarations

Ethical Consideration for animal studies

All procedures related to animal handling, care, surgery, and sacrifice were approved by the Institutional Animal Care and Use Committee of Kindai University as the approved research project number KAME2024-039 and performed in accordance with institutional guidelines and regulations. All methods are reported in accordance with ARRIVE guidelines.

Author Contributions and consent for publication

K.T.: provision of study material, collection and/or assembly of data, data analysis and interpretation, manuscript writing, final approval of manuscript; S.M.: data analysis and interpretation, manuscript writing, final approval of manuscript; T.M.: collection and/or assembly of data, data analysis and interpretation. T.H.: preparation of materials, final approval of manuscript; T.T.: collection and/or assembly of data, final approval of manuscript; K.G.: data analysis and interpretation, final approval of manuscript; A.I.: conception and design, collection and/or assembly of data, data analysis and

interpretation; T. Teramura.: conception and design, collection and/or assembly of data, data analysis and interpretation, manuscript writing, and final approval of manuscript.

Disclosure of Potential Conflicts of Interest

The authors indicated no potential conflicts of interest.

Funding

This research was supported by MEXT/JSPS KAKENHI Grant-in-Aid for Young Scientists (B) Grant 26K19891 (Kensuke Toriumi), and the Kindai University Research Grants KD-2601 for Takeshi Teramura and SR-07 for Kensuke Toriumi.

Author Contribution

K.T.: provision of study material, collection and/or assembly of data, data analysis and interpretation, manuscript writing, final approval of manuscript; A.I.: conception and design, collection and/or assembly of data, data analysis and interpretation; T.M.: collection and/or assembly of data, data analysis and interpretation; T.H.: preparation of materials, final approval of manuscript; S.M.: data analysis and interpretation, manuscript writing, final approval of manuscript; T.T.: collection and/or assembly of data, final approval of manuscript; K.G.: data analysis and interpretation, final approval of manuscript; T. Teramura.: conception and design, collection and/or assembly of data, data analysis and interpretation, manuscript writing, and final approval of manuscript.All authors reviewed the manuscript.

Data Availability

The data that support the findings of this study are available from the corresponding author upon reasonable request. The microarray data generated in this study are available in the Gene Expression Omnibus repository under accession number GSE352598.

References

1. Wang S, Chen S, Fan W, Chen T, Hu X, Li C, Wu Z, Xu W, Xiao Z, Ma B, Cheng L: Global Inequalities in the Burden of Traumatic Spinal Cord Injury from 1990 to 2021: Findings from the Global Burden of Disease Study 2021. *Neuroepidemiology* 2026, 60:817–835.
2. Kjell J, Dulin JN, Warren PM: Editorial: Fighting for recovery on multiple fronts in spinal cord injury. *Front Cell Neurosci* 2023, 17:1178192.
3. Gazdic M, Volarevic V, Harrell CR, Fellabaum C, Jovicic N, Arsenijevic N, Stojkovic M: Stem Cells Therapy for Spinal Cord Injury. *Int J Mol Sci* 2018, 19.

4. Montoto-Marques A, Benito-Penalva J, Ferreiro-Velasco ME, Andrew Wright M, Salvador-De la Barrera S, Kumru H, Gaitan-Perez N, Hernandez-Navarro A, Rodriguez-Sotillo A, Martins Braga F, et al: Advances and New Therapies in Traumatic Spinal Cord Injury. *J Clin Med* 2025, 14.
5. Montoto-Meijide R, Meijide-Failde R, Diaz-Prado SM, Montoto-Marques A: Mesenchymal Stem Cell Therapy in Traumatic Spinal Cord Injury: A Systematic Review. *Int J Mol Sci* 2023, 24.
6. Xia Y, Zhu J, Yang R, Wang H, Li Y, Fu C: Mesenchymal stem cells in the treatment of spinal cord injury: Mechanisms, current advances and future challenges. *Front Immunol* 2023, 14:1141601.
7. Wang R, Wang Y, Yan F, Sun J, Zhang T: Assessment of mesenchymal stem cells for the treatment of spinal cord injury: a systematic review and network meta-analysis. *Front Cell Neurosci* 2025, 19:1532219.
8. Honmou O, Yamashita T, Morita T, Oshigiri T, Hirota R, Iyama S, Kato J, Sasaki Y, Ishiai S, Ito YM, et al: Intravenous infusion of auto serum-expanded autologous mesenchymal stem cells in spinal cord injury patients: 13 case series. *Clin Neurol Neurosurg* 2021, 203:106565.
9. Nakajima H, Uchida K, Guerrero AR, Watanabe S, Sugita D, Takeura N, Yoshida A, Long G, Wright KT, Johnson WE, Baba H: Transplantation of mesenchymal stem cells promotes an alternative pathway of macrophage activation and functional recovery after spinal cord injury. *J Neurotrauma* 2012, 29:1614–1625.
10. Brockie S, Hong J, Fehlings MG: The Role of Microglia in Modulating Neuroinflammation after Spinal Cord Injury. *Int J Mol Sci* 2021, 22.
11. Hakim R, Zachariadis V, Sankavaram SR, Han J, Harris RA, Brundin L, Enge M, Svensson M: Spinal Cord Injury Induces Permanent Reprogramming of Microglia into a Disease-Associated State Which Contributes to Functional Recovery. *J Neurosci* 2021, 41:8441–8459.
12. Butovsky O, Jedrychowski MP, Moore CS, Cialic R, Lanser AJ, Gabriely G, Koeglsperger T, Dake B, Wu PM, Doykan CE, et al: Identification of a unique TGF-beta-dependent molecular and functional signature in microglia. *Nat Neurosci* 2014, 17:131–143.
13. Bedolla A, Wegman E, Weed M, Stevens MK, Ware K, Paranjpe A, Alkhimovitch A, Ifergan I, Taranov A, Peter JD, et al: Adult microglial TGFbeta1 is required for microglia homeostasis via an autocrine mechanism to maintain cognitive function in mice. *Nat Commun* 2024, 15:5306.
14. Noh MY, Lim SM, Oh KW, Cho KA, Park J, Kim KS, Lee SJ, Kwon MS, Kim SH: Mesenchymal Stem Cells Modulate the Functional Properties of Microglia via TGF-beta Secretion. *Stem Cells Transl Med* 2016, 5:1538–1549.
15. Toriumi K, Onodera Y, Takehara T, Mori T, Hasei J, Shigi K, Iwawaki N, Ozaki T, Akagi M, Nakanishi M, Teramura T: LRRC15 expression indicates high level of stemness regulated by TWIST1 in mesenchymal stem cells. *iScience* 2023, 26:106946.
16. Mass E, Ballesteros I, Farlik M, Halbritter F, Gunther P, Crozet L, Jacome-Galarza CE, Handler K, Klughammer J, Kobayashi Y, et al: Specification of tissue-resident macrophages during organogenesis. *Science* 2016, 353.

17. Sanjurjo L, Aran G, Tellez E, Amezaga N, Armengol C, Lopez D, Prats C, Sarrias MR: CD5L Promotes M2 Macrophage Polarization through Autophagy-Mediated Upregulation of ID3. *Front Immunol* 2018, 9:480.
18. Buss A, Pech K, Kakulas BA, Martin D, Schoenen J, Noth J, Brook GA: TGF-beta1 and TGF-beta2 expression after traumatic human spinal cord injury. *Spinal Cord* 2008, 46:364–371.
19. Jiang Y, McLennan IS, Koishi K, Hendry IA: Transforming growth factor-beta 2 is anterogradely and retrogradely transported in motoneurons and up-regulated after nerve injury. *Neuroscience* 2000, 97:735–742.
20. Jiang Y, Zhang M, Koishi K, McLennan IS: TGF-beta 2 attenuates the injury-induced death of mature motoneurons. *J Neurosci Res* 2000, 62:809–813.
21. Peterziel H, Unsicker K, Krieglstein K: TGFbeta induces GDNF responsiveness in neurons by recruitment of GFRalpha1 to the plasma membrane. *J Cell Biol* 2002, 159:157–167.
22. Logan A, Green J, Hunter A, Jackson R, Berry M: Inhibition of glial scarring in the injured rat brain by a recombinant human monoclonal antibody to transforming growth factor-beta2. *Eur J Neurosci* 1999, 11:2367–2374.
23. Moon LD, Fawcett JW: Reduction in CNS scar formation without concomitant increase in axon regeneration following treatment of adult rat brain with a combination of antibodies to TGFbeta1 and beta2. *Eur J Neurosci* 2001, 14:1667–1677.
24. King VR, Phillips JB, Brown RA, Priestley JV: The effects of treatment with antibodies to transforming growth factor beta1 and beta2 following spinal cord damage in the adult rat. *Neuroscience* 2004, 126:173–183.
25. Ueno M, Fujita Y, Tanaka T, Nakamura Y, Kikuta J, Ishii M, Yamashita T: Layer V cortical neurons require microglial support for survival during postnatal development. *Nat Neurosci* 2013, 16:543–551.
26. Wlodarczyk A, Holtman IR, Krueger M, Yogev N, Bruttger J, Khorooshi R, Benmamar-Badel A, de Boer-Bergsma JJ, Martin NA, Karram K, et al: A novel microglial subset plays a key role in myelinogenesis in developing brain. *EMBO J* 2017, 36:3292–3308.
27. Zhou Z, Peng X, Insolera R, Fink DJ, Mata M: Interleukin-10 provides direct trophic support to neurons. *J Neurochem* 2009, 110:1617–1627.
28. Cafferty WB, Gardiner NJ, Das P, Qiu J, McMahon SB, Thompson SW: Conditioning injury-induced spinal axon regeneration fails in interleukin-6 knock-out mice. *J Neurosci* 2004, 24:4432–4443.
29. Boulenguez P, Liabeuf S, Bos R, Bras H, Jean-Xavier C, Brocard C, Stil A, Darbon P, Cattaert D, Delpire E, et al: Down-regulation of the potassium-chloride cotransporter KCC2 contributes to spasticity after spinal cord injury. *Nat Med* 2010, 16:302–307.
30. Coull JA, Beggs S, Boudreau D, Boivin D, Tsuda M, Inoue K, Gravel C, Salter MW, De Koninck Y: BDNF from microglia causes the shift in neuronal anion gradient underlying neuropathic pain. *Nature* 2005, 438:1017–1021.

31. Hains BC, Waxman SG: Activated microglia contribute to the maintenance of chronic pain after spinal cord injury. *J Neurosci* 2006, 26:4308–4317.
32. Yousefifard M, Nasirinezhad F, Shardi Manaheji H, Janzadeh A, Hosseini M, Keshavarz M: Human bone marrow-derived and umbilical cord-derived mesenchymal stem cells for alleviating neuropathic pain in a spinal cord injury model. *Stem Cell Res Ther* 2016, 7:36.

Figures

Figure 1

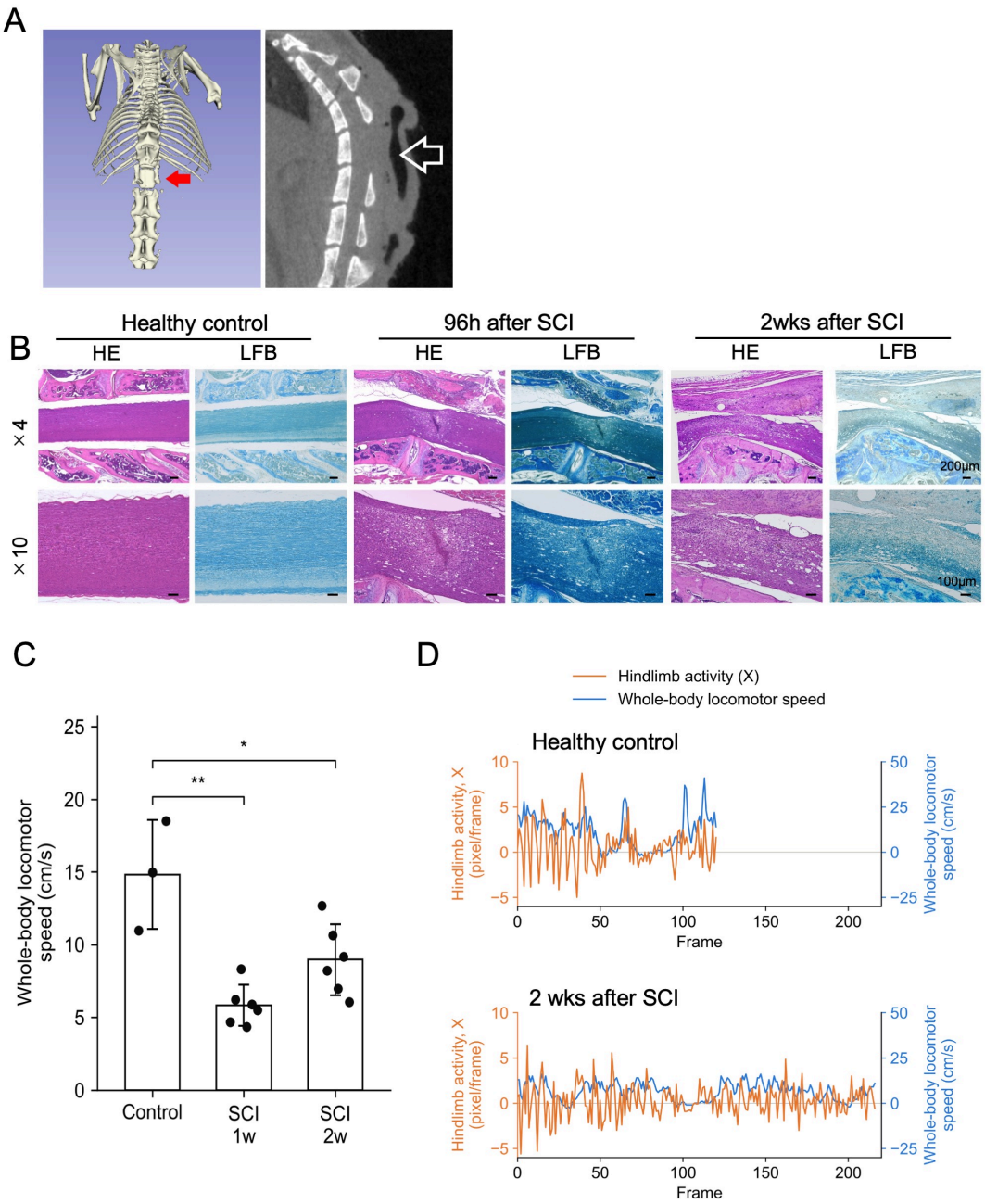

Figure 1

A spinal cord injury model produced by briefly clipping with forceps.

(A) Micro-CT confirmation of the partial laminectomy. Left, three-dimensional reconstruction of the spine (dorsal view). Right, sagittal section of the spine. The red arrow and the open arrow both indicate the laminectomy site at L1.

(B) Histological changes at the lesion site in this SCI model. Sagittal sections of the healthy spinal cord and of the injured cord at 96 h and 2 wk after injury were stained with hematoxylin and eosin (H&E) and Luxol Fast Blue (LFB). Upper panels, low magnification; lower panels, high magnification. Tissue disruption with hemorrhage is seen at the lesion center at 96 h, and demyelination with reduced LFB staining is seen at 2 wk.

(C) Whole-body locomotor speed after SCI. Whole-body locomotor speed of control mice and of SCI mice at 1 and 2 weeks after injury. Speed was calculated for each mouse as the mean velocity of frames in which forward body movement was ≥2 cm/s. Bars show mean ± SD, and dots show individual mice (Control, n = 3; SCI, n = 6, with the same animals assessed at 1 and 2 weeks). *P < 0.05, **P < 0.01, one-way ANOVA followed by Tukey's test.

(D) Representative time series of the forward (X) component of hindlimb movement (orange, left axis; pixel/frame) and whole-body locomotor speed (blue, right axis; cm/s) in a healthy control mouse and a mouse 2 wk after SCI

Figure 2

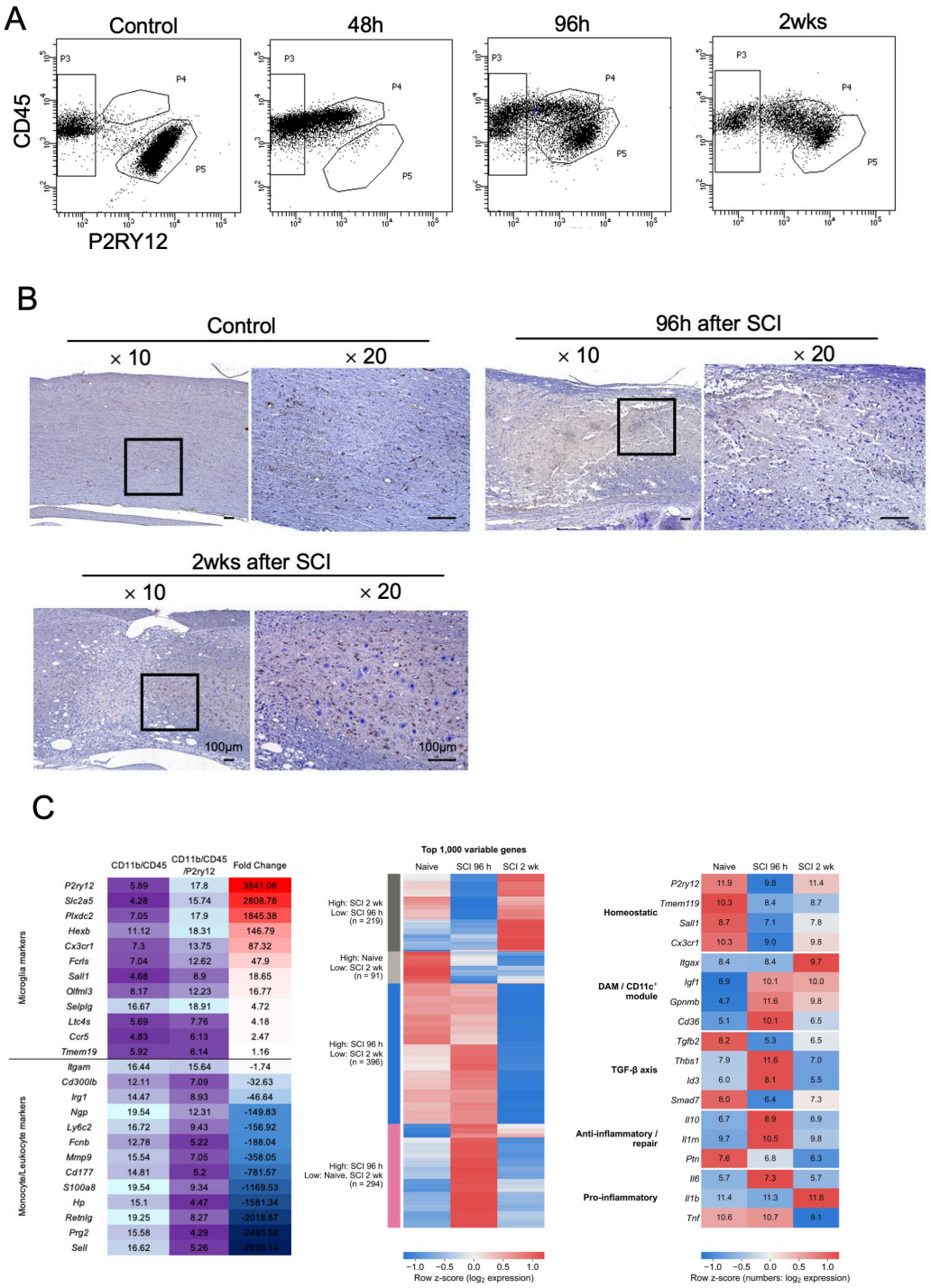

Figure 2

SCI transiently shifts microglia to an activated state and subsequently drives a DAM-like phenotype

(A) Flow cytometric comparison of three CD11b⁺ fractions: naïve (homeostatic) microglia (CD11b⁺CD45^{low}P2RY12⁺), intermediate- and activated microglia (DAM, CD11b⁺CD45^{high} P2RY12⁺), and monocyte derived macrophage (MDM) and activated microglia-enriched fraction (CD11b⁺CD45^{high}

P2RY12⁻), which also contains infiltrating macrophages. SCI reduced the homeostatic microglia fraction and increased the activated microglia-enriched fraction.

(B) P2RY12 immunohistochemistry of sagittal spinal cord sections from a healthy control mouse and from mice 96 h and 2 wk after SCI. Left, low-magnification images (10× objective); right, higher-magnification images (20× objective) of the boxed areas in the left panels. At 96 h, P2RY12⁺ cells accumulated near the lesion; at 2 wk, they were diffusely distributed around the demyelinated area.

(C) Microarray analysis of CD11b⁺CD45low P2RY12⁺ microglia. **Left:** Comparison of the CD11b⁺CD45⁺ and CD11b⁺CD45low P2RY12⁺ fractions from healthy mice. The CD11b⁺CD45low P2RY12⁺ fraction showed a typical homeostatic microglial profile, with high expression of microglial markers and low expression of monocyte/leukocyte markers. Values are log2 expression and fold change. **Middle:** Hierarchical clustering of the 1,000 most variable genes across healthy, SCI 96 h and SCI 2 wk samples (row z-score). The bar on the left indicates gene clusters defined by expression pattern. **Right:** Expression of functional gene modules (homeostatic, DAM/CD11c⁺, TGF-β axis, anti-inflammatory/repair, pro-inflammatory). Colors show row z-scores; numbers show log2 expression.

Figure 3

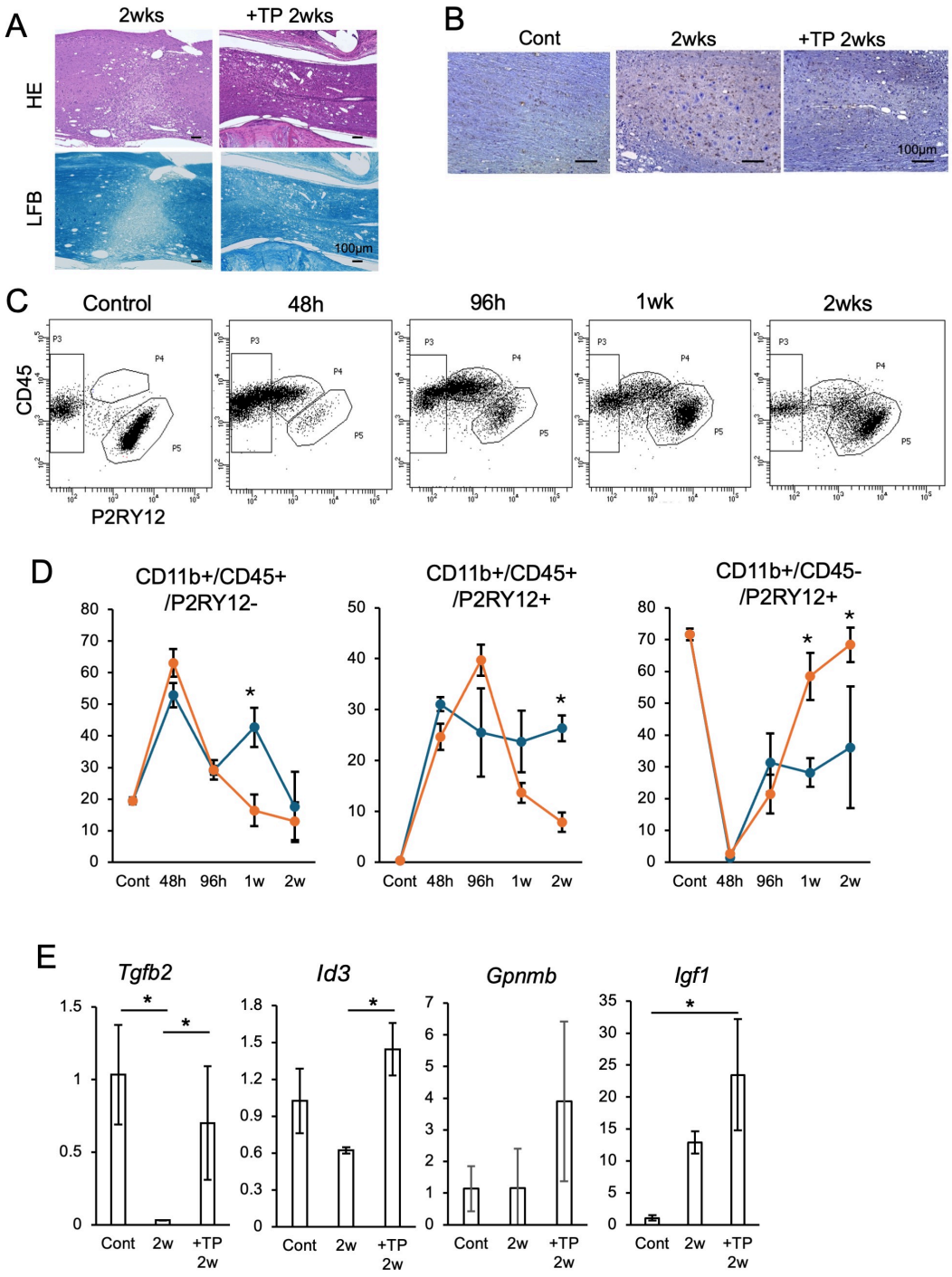

Figure 3

MSC transplantation accelerates the return of microglia to a homeostatic state and restores Tgfb2 expression after SCI.

(A) Demyelination after MSC sheet transplantation. Representative sagittal sections of the spinal cord 2 wk after SCI without transplantation (left) and 2 wk after SCI with simultaneous MSC sheet

transplantation (+TP; right), stained with H&E (upper) and LFB (lower). In the untreated SCI cord, LFB staining was lost across the full dorsoventral extent of the lesion, whereas in the transplanted cord LFB staining was relatively preserved and no full-thickness demyelination was observed.

(B) P2RY12 immunohistochemistry in healthy controls (Cont), at 2 wk after SCI without transplantation (2wks) and at 2 wk after SCI with MSC sheet transplantation (+TP 2wks). Representative images near the lesion are shown. In all three groups, DAB-positive (brown) $P2RY12^{+}$ cells were distributed throughout the field. Counterstained with hematoxylin.

(C) Time course of microglial fractions after MSC transplantation analyzed by flow cytometry. Representative CD45 versus P2RY12 plots of $CD11b^{+}$ cells from a healthy control and from mice 48 h, 96 h, 1 wk and 2 wk after SCI with simultaneous MSC sheet transplantation. Numbers indicate the percentage of cells in each gate. The time course without transplantation is shown in Figure 2A.

(D) Time course of the proportion of each fraction gated in Figure 3C: homeostatic microglia ($CD11b^{+}CD45^{low}P2RY12^{+}$), intermediate microglia ($CD11b^{+}CD45^{high}$ $P2RY12^{+}$) and the activated microglia-enriched fraction ($CD11b^{+}CD45^{high}$ $P2RY12^{-}$). The y-axis shows the percentage of $CD11b^{+}$ cells. (n = 3, mean ± SD)

(E) qPCR analysis of Tgfb2, Id3, Gpnmb and Igf1 in sorted $CD11b^{+}CD45^{low}$ $P2RY12^{+}$ cells from healthy controls (Cont), mice 2 wk after SCI (2w) and mice 2 wk after SCI with MSC sheet transplantation (+TP 2w). Expression was normalized to *Actinb* and shown relative to Cont. Mean ± SD; n = 3 per group. *P < 0.05 (one-way ANOVA followed by Tukey's test).

Figure 4

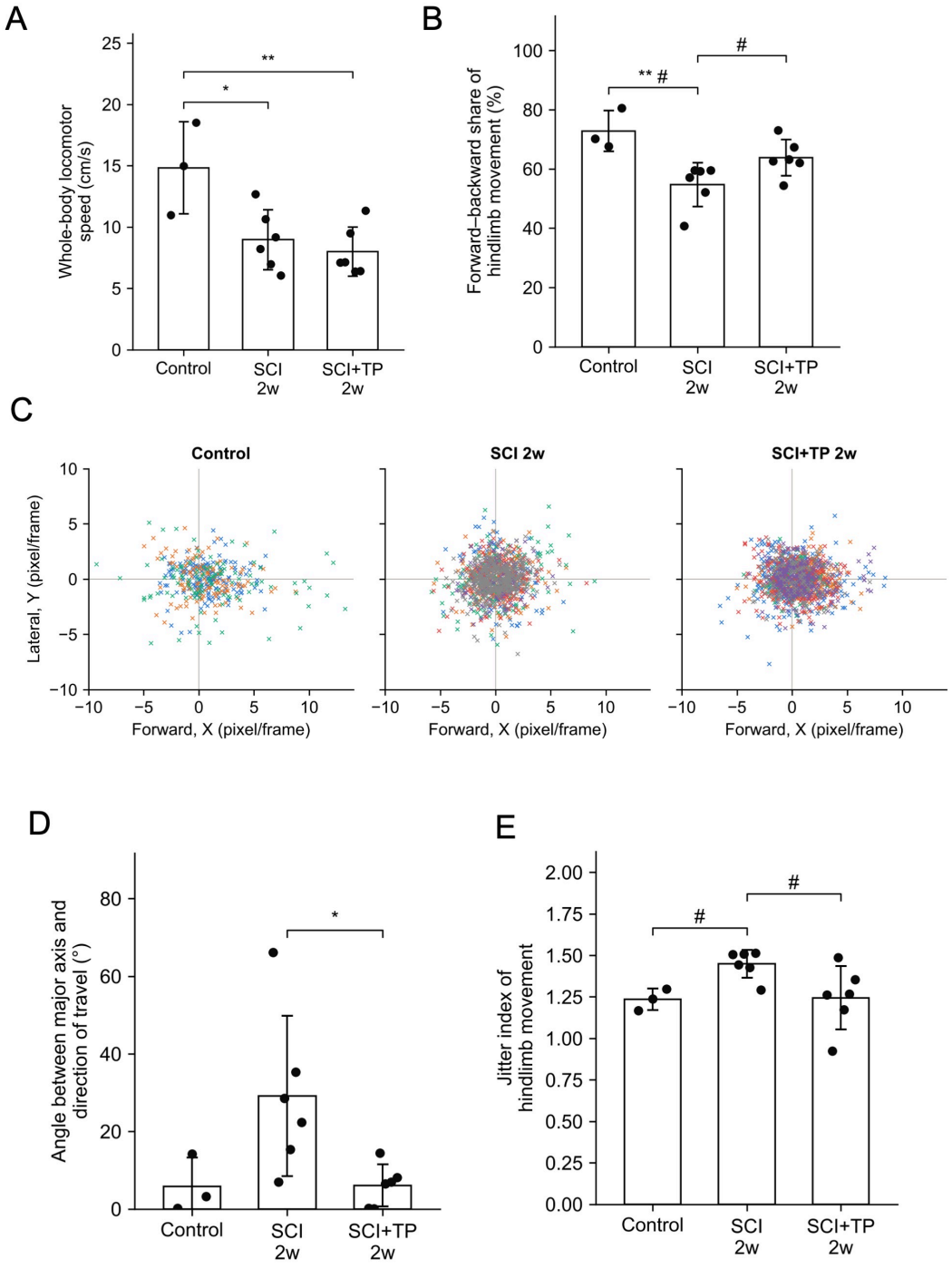

Figure 4

MSC transplantation restores hindlimb movement directionality after SCI.
Hindlimb and whole-body movement of control, SCI, and SCI+TP mice at 2 weeks after injury. **(A)**Whole-body locomotor speed. **(B)**Forward–backward share of hindlimb movement. **(C)** Frame-by-frame hindlimb displacement vectors after removal of whole-body motion; X, direction of travel (forward positive); Y, lateral (pixel/frame). Each mark represents one frame, and colors indicate individual mice.

(D) Angle between the major axis of the hindlimb vector distribution and the direction of travel. **(E)**Jitter index of the forward hindlimb component. In A, B, D, and E, bars show mean ± SD and dots show individual mice (Control, n = 3; SCI, n = 6; SCI+TP, n = 6). *P < 0.05, **P < 0.01, one-way ANOVA followed by Tukey's test; #P < 0.05, planned comparisons (Control vs SCI and SCI vs SCI+TP) by two-sided Welch's t-test with Holm correction. Definitions of all indices are given in Methods.

Supplementary Files

This is a list of supplementary files associated with this preprint. Click to download.

- Supplementarytable.docx
- Sup2.jpeg
- Sup1.jpeg